Toward optimal LES on unstructured meshes

By A. Haselbacher †, R.D. Moser ‡, G. Constantinescu AND K. Mahesh ¶

A new approach for determining the correlation data required by the optimal-LES procedure of Langford and Moser (Optimal LES formulations for isotropic turbulence, *J. Fluid Mech.*, **398**, 321–346, 1999) is presented. Based on Kolmogorov's theory for isotropic turbulence, the new approach leads to stencil coefficients in terms of integrated multi-point correlations. The explicit dependence of the optimal-LES method on DNS data is thus eliminated, and its applicability is extended to high Reynolds-number flows in complex geometries. A preliminary verification of the new optimal-LES method for decaying isotropic turbulence showed good results for decay rates.

1. Introduction and Motivation

Large-Eddy Simulation (LES) is a computational technique for turbulent flows in which only large scales are resolved and the effect of the unresolved small scales is modeled. The reduced resolution makes LES an attractive approach for the analysis of engineering applications, in which the large scales often dominate momentum and heat transfer.

The separation of scales is commonly achieved through a filter operator. The lack of an unambiguous separation of the resolved and modeled scales leads to many challenging issues, including: the precise definition of the filter operator, the construction of accurate numerical methods, and, for inhomogeneous flows, the formulation of subgrid-scale models and the presence of commutation errors. These issues often involve both numerical and physical aspects and it can be difficult to isolate their effects with certainty and generality.

In an effort to address these issues, Langford & Moser (1999) introduced the concept of an "ideal LES" which is the best possible approximation, given that filtering incurs a loss of information. The ideal LES, based on the conditional average, can be proved to yield accurate large-scale one-time statistics and to minimize the error of large-scale short-time dynamics. However, the conditional average defining the ideal LES is impractical to compute because the condition is on the entire LES field. To reduce the computational cost to a practical level, the conditional average is approximated using stochastic estimation, see Adrian (1995), resulting in an approximation to the ideal LES called "optimal LES".

The optimal-LES technique was applied to forced isotropic turbulence at $\mathrm{Re}_\lambda = 164$ by Langford & Moser (1999) and to turbulent channel flow at $\mathrm{Re}_\tau = 587$ by Völker (2000). In these computations, the correlations required by the stochastic-estimation procedure were determined from Direct Numerical Simulation (DNS) data. This places an undesirable restriction on optimal LES because DNS data is available only at relatively low Reynolds numbers and for simple geometries.

† Center for Simulation of Advanced Rockets, University of Illinois at Urbana-Champaign
‡ Theoretical and Applied Mechanics, University of Illinois at Urbana-Champaign
¶ Aerospace Engineering and Mechanics, University of Minnesota

The goal of the present work is to extend the applicability of optimal LES to high-Reynolds number flows and to complex geometries. To achieve this goal, we propose a new approach in which the correlations required by the stochastic-estimation procedure are computed from turbulence theory. This approach was demonstrated for a model equation in one dimension by Balakrishnan & Moser (2001). More specifically, the present work extends the optimal-LES method to formally infinitely high Reynolds numbers by using results from Kolmogorov's theory for isotropic turbulence. This article describes this extension and presents results of a preliminary verification on unstructured grids.

The remainder of the article is structured as follows: Section 2 describes the finite-volume optimal-LES approach and explains the determination of the stencil weights using isotropic turbulence theory. The computational approach is outlined in section 3, which includes a description of the implementation of the finite-volume optimal-LES method on unstructured grids. Results are presented and discussed in section 4. Conclusions are drawn in section 5.

2. Finite-volume optimal-LES formulation

The finite-volume optimal-LES formulation was originally developed by Langford (2000) and is outlined in subsections 2.1 and 2.2. The current formulation is restricted to incompressible flows. The new approach of obtaining the correlation data from Kolmogorov's theory of isotropic turbulence is described in subsection 2.3.

2.1. *Theoretical formulation*

For incompressible flow, the momentum equations can be expressed in integral form as

$$\Delta^3 \frac{\mathrm{d}w_i}{\mathrm{d}t} + \int_s u_i u_s \, d\mathbf{x} = -\int_s p n_i \, d\mathbf{x} + \int_s \nu \frac{\partial u_i}{\partial x_j} n_j \, d\mathbf{x}, \tag{2.1}$$

where the cell-averaged velocity is defined by

$$w_i = \frac{1}{\Delta^3} \int_v u_i(\mathbf{x}) \, d\mathbf{x}, \tag{2.2}$$

and $u_s = u_i n_i$ is the velocity along the outward-directed unit normal vector with components n_i, the density has been absorbed into the pressure, ν is the kinematic viscosity, and $\mathbf{x} = \{x_1, x_2, x_3\}^t$ is the position vector. The volume of the integration region is denoted by Δ^3, so that Δ may be interpreted as the cell width for uniform hexahedral grids. The subscripts s and v indicate surface and volume integrals, respectively.

In the finite-volume optimal-LES method, the cell-averaging defined by (2.2) is regarded as the filtering operation. It is assumed that the filter width is in the inertial range. In the following, w_i and u_i are referred to as filtered and unfiltered values, respectively.

To evolve the filtered values, the fluxes of unfiltered variables appearing in (2.1) must be expressed in terms of filtered values. Thus the flux is estimated in terms of a quadratic expression of the filtered values,

$$\begin{aligned} \int_s u_i(\mathbf{x}) u_s(\mathbf{x}) \, d\mathbf{x} = &\sum_v L_{ij}(s, v) \int_v u_j(\mathbf{x}) \, d\mathbf{x} \\ &+ \sum_{v_1, v_2} Q_{ijk}(s, v_1, v_2) \int_{v_1} u_j(\mathbf{x}^1) \, d\mathbf{x}^1 \int_{v_2} u_k(\mathbf{x}^2) \, d\mathbf{x}^2, \end{aligned} \tag{2.3}$$

where the functional dependences of the velocity components were added to indicate the surfaces and volumes over which they are integrated.

Before addressing the determination of the estimation coefficients L and Q—which may also be interpreted as stencil weights—we draw attention to the following point: in contrast to conventional LES approaches, (2.1) is not space-filtered independently of the numerical discretization, the fluxes are not cast in terms of filtered values, and we do not explicitly define a subgrid-scale term. Instead, the optimal-LES method approximates the combination of fluxes and subgrid effects in an optimal way. The reasoning is that conventional finite-volume methods evaluate fluxes based on approximations derived from Taylor-series expansions, and thus require the cells to be small compared to characteristic length scales of the underlying functions. This requirement is violated in LES, so the definition of subgrid effects depends on the order of the flux approximation.

2.2. *Stencil-weights construction*

To determine the unknown stencil weights L and Q, we take moments of (2.3) and ensemble-average to obtain the system of equations,

$$I^1_{li}(v',s) = \sum_v L_{ij}(s,v) I^2_{lj}(v',v) + \sum_{v_1,v_2} Q_{ijk}(s,v_1,v_2) I^3_{ljk}(v',v_1,v_2) \tag{2.4}$$

$$I^4_{lmi}(v'_1,v'_2,s) = \sum_v L_{ij}(s,v) I^3_{lmj}(v'_1,v'_2,v) + \sum_{v_1,v_2} Q_{ijk}(s,v_1,v_2) I^5_{lmjk}(v'_1,v'_2,v_1,v_2) \tag{2.5}$$

where the integrated correlations I^1 to I^5 are given by,

$$I^1_{li}(v',s) = \int_{v'}\int_s \langle u_l(\mathbf{x}')u_i(\mathbf{x})u_s(\mathbf{x})\rangle \, d\mathbf{x}\, d\mathbf{x}' \tag{2.6}$$

$$I^2_{lj}(v',v) = \int_{v'}\int_v \langle u_l(\mathbf{x}')u_j(\mathbf{x})\rangle \, d\mathbf{x}\, d\mathbf{x}' \tag{2.7}$$

$$I^3_{ljk}(v',v_1,v_2) = \int_{v'}\int_{v_1}\int_{v_2} \langle u_l(\mathbf{x}')u_j(\mathbf{x}^1)u_k(\mathbf{x}^2)\rangle \, d\mathbf{x}^2\, d\mathbf{x}^1\, d\mathbf{x}' \tag{2.8}$$

$$I^4_{lmi}(v'_1,v'_2,s) = \int_{v'_1}\int_{v'_2}\int_s \langle u_l(\mathbf{x}^{1\prime})u_m(\mathbf{x}^{2\prime})u_i(\mathbf{x})u_s(\mathbf{x})\rangle \, d\mathbf{x}\, d\mathbf{x}^{2\prime}\, d\mathbf{x}^{1\prime} \tag{2.9}$$

$$I^5_{lmjk}(v'_1,v'_2,v_1,v_2) = \int_{v'_1}\int_{v'_2}\int_{v_1}\int_{v_2} \langle u_l(\mathbf{x}^{1\prime})u_m(\mathbf{x}^{2\prime})u_j(\mathbf{x}^1)u_k(\mathbf{x}^2)\rangle \, d\mathbf{x}^2\, d\mathbf{x}^1\, d\mathbf{x}^{2\prime}\, d\mathbf{x}^{1\prime} \tag{2.10}$$

Thus, three correlation tensors are needed to determine the estimation coefficients,

$$R_{ij}(\mathbf{r}^1) = \langle u_i(\mathbf{x})u_j(\mathbf{x}^1)\rangle, \tag{2.11}$$

$$T_{ijk}(\mathbf{r}^1,\mathbf{r}^2) = \langle u_i(\mathbf{x})u_j(\mathbf{x}^1)u_k(\mathbf{x}^2)\rangle, \tag{2.12}$$

$$F_{ijkl}(\mathbf{r}^1,\mathbf{r}^2,\mathbf{r}^3) = \langle u_i(\mathbf{x})u_j(\mathbf{x}^1)u_k(\mathbf{x}^2)u_l(\mathbf{x}^3)\rangle, \tag{2.13}$$

where homogeneity was assumed in order to express the correlations in terms of separation vectors $\mathbf{r}^i = \mathbf{x} - \mathbf{x}^i$.

2.3. *Determination of correlations*

To determine the correlations given by (2.11)-(2.13), the spatial separations are assumed to be small enough to be in the Kolmogorov inertial range of isotropic turbulence at an infinite Reynolds number. Thus the correlations are represented by isotropic tensors, and

we use the expressions for the second- and third-order longitudinal structure functions,

$$S_2(r^1) = \langle (u_\parallel(\mathbf{x}) - u_\parallel(\mathbf{x}^1))^2 \rangle = C_1 \epsilon^{2/3} (r^1)^{2/3}, \tag{2.14}$$

$$S_3(r^1) = \langle (u_\parallel(\mathbf{x}) - u_\parallel(\mathbf{x}^1))^3 \rangle = -\frac{4}{5} \epsilon r^1, \tag{2.15}$$

where $r^i = ||\mathbf{r}^i||$ is the magnitude of the separation vector, $u_\parallel$ is the velocity component in the direction of the separation vector, ϵ is the rate of dissipation of turbulence kinetic energy, and $C_1 \approx 2.0$ is the Kolmogorov constant.

2.3.1. *Two-point second-order correlation*

The two-point second-order correlation is given by the well-known expression

$$R_{ij}(\mathbf{r}^1) = u^2 \left[f \delta_{ij} + \frac{1}{2} r f' \left(\delta_{ij} - \frac{r^1_i r^1_j}{(r^1)^2} \right) \right], \tag{2.16}$$

where u^2 is the variance, $f(r^1) = \langle u_{||}(\mathbf{x}) u_{||}(\mathbf{x} + \mathbf{r}^1) \rangle / u^2$ is the longitudinal correlation coefficient, and δ_{ij} is the Kronecker delta. The longitudinal correlation coefficient can be determined from (2.14), which allows (2.16) to be rewritten as

$$R_{ij}(\mathbf{r}^1) = u^2 \delta_{ij} + \frac{C_1}{6} \epsilon^{2/3} (r^1)^{2/3} \left(\frac{r^1_i r^1_j}{(r^1)^2} - 4 \delta_{ij} \right), \tag{2.17}$$

and hence I^2 can be computed.

2.3.2. *Two-point third-order correlation*

The most general isotropic third-order tensor which satisfies the continuity constraint and is symmetric with respect to exchanging the i and j indices is given by

$$T_{ijk}(0, \mathbf{r}^1) = h \delta_{ij} \frac{r^1_k}{r^1} - \left(\frac{r^1 h'}{2} + h \right) \left(\delta_{ik} \frac{r^1_j}{r^1} + \delta_{jk} \frac{r^1_i}{r^1} \right) + (r^1 h' - h) \frac{r^1_i r^1_j r^1_k}{(r^1)^3}, \tag{2.18}$$

where $h(r^1) = \langle u^2_{||}(\mathbf{x}) u_{||}(\mathbf{x} + \mathbf{r}^1) \rangle / u^3$ is the longitudinal correlation coefficient. By considering the tensor

$$B_{ijk}(\mathbf{r}^1) = \left\langle \left(u_i(\mathbf{x}^1) - u_i(\mathbf{x}) \right) \left(u_j(\mathbf{x}^1) - u_j(\mathbf{x}) \right) \left(u_k(\mathbf{x}^1) - u_k(\mathbf{x}) \right) \right\rangle \tag{2.19}$$

$$= 2 \left(T_{ijk}(0, \mathbf{r}^1) + T_{ikj}(0, \mathbf{r}^1) + T_{jki}(0, \mathbf{r}^1) \right), \tag{2.20}$$

it can be shown that

$$S_3(r^1) = B_{ijk}(\mathbf{r}^1) \frac{r^1_i r^1_j r^1_k}{r^1} = -12 h(r^1). \tag{2.21}$$

Having expressed $h(r^1)$ in terms of the third-order longitudinal structure function, (2.15) can be recast as

$$T_{ijk}(0, \mathbf{r}^1) = \frac{\epsilon}{15} \left[\delta_{ij} r^1_k - \frac{3}{2} \left(\delta_{ik} r^1_j + \delta_{jk} r^1_i \right) \right], \tag{2.22}$$

from which I^1 can be computed.

2.3.3. *Three-point third-order correlation*

We have so far been unable to find or derive an expression for the three-point third-order correlation. Fortunately, we can circumvent this issue by computing I^3 directly

from filtered data as

$$I^3_{ljk}(v', v_1, v_2) = \left\langle \int_{v'} u_l(\mathbf{x}')\, d\mathbf{x}' \int_{v_1} u_j(\mathbf{x}^1)\, d\mathbf{x}^1 \int_{v_2} u_k(\mathbf{x}^2)\, d\mathbf{x}^2 \right\rangle \tag{2.23}$$

$$= \left\langle w_l(\mathbf{x}') w_j(\mathbf{x}^1) w_k(\mathbf{x}^2) \right\rangle . \tag{2.24}$$

We thus propose to compute I^3 dynamically during the calculation from cell-averaged data. Note that this approach can in principle be applied to all pure volume integrals.

In (2.24) and all subsequent expressions involving averages of cell-averaged values, the angled brackets denote a volume average.

2.3.4. *Fourth-order correlations*

The quasi-normal approximation is invoked to determine the fourth-order correlations. The fourth-order correlations are thus expressed in terms of the second-order two-point correlations as

$$F_{ijkl}(\mathbf{r}^1, \mathbf{r}^2, \mathbf{r}^3) = R_{ij}(\mathbf{r}^1) R_{kl}(\mathbf{r}^3 - \mathbf{r}^2) + R_{ik}(\mathbf{r}^2) R_{jl}(\mathbf{r}^3 - \mathbf{r}^1) + R_{il}(\mathbf{r}^3) R_{jk}(\mathbf{r}^2 - \mathbf{r}^1). \tag{2.25}$$

Hence I^4 and I^5 can be determined from (2.25) and (2.17).

2.4. *Scaling of integrated correlations*

The integrated correlations depend on the geometric configuration of the volumes over which they are integrated, and on the flow solution via u^2 and ϵ. These dependencies can be parameterized through a scaling. However, because of the existence of two length scales, i.e., the filter width Δ and the energy-containing length scale u^3/ϵ, not all the quantities are scaled consistently.

Based on the forms of the various approximations to the correlations, the following scaled quantities are defined (dependencies and subscripts are suppressed for simplicity of notation):

$$\tilde{I}^1 = \frac{I^1}{\epsilon \Delta^6}, \tag{2.26}$$

$$\tilde{I}^2 = \frac{I^2}{u^2 \Delta^6}, \tag{2.27}$$

$$\tilde{I}^3 = \frac{I^3}{\epsilon \Delta^{10}}, \tag{2.28}$$

$$\tilde{I}^4 = \frac{I^4}{u^4 \Delta^8}, \tag{2.29}$$

$$\tilde{I}^5 = \frac{I^5}{u^4 \Delta^{12}}, \tag{2.30}$$

$$\tilde{L} = \frac{L u^2}{\epsilon}, \tag{2.31}$$

$$\tilde{Q} = Q \Delta^4. \tag{2.32}$$

Then (2.4) and (2.5) can be rewritten as

$$\tilde{I}^1_{li}(v', s) = \sum_v \tilde{L}_{ij}(s, v) \tilde{I}^2_{lj}(v', v) + \sum_{v_1, v_2} \tilde{Q}_{ijk}(s, v_1, v_2) \tilde{I}^3_{ljk}(v', v_1, v_2) \tag{2.33}$$

$$\tilde{I}^4_{lmi}(v'_1, v'_2, s) = \lambda^2 \sum_v \tilde{L}_{ij}(s, v) \tilde{I}^3_{lmj}(v'_1, v'_2, v) + \sum_{v_1, v_2} \tilde{Q}_{ijk}(s, v_1, v_2) \tilde{I}^5_{lmjk}(v'_1, v'_2, v_1, v_2) \tag{2.34}$$

where $\lambda = \Delta\epsilon/u^3$, the ratio of the filter width to the large turbulence length scale, will generally be small. In the limit $\lambda \to 0$, Q can be determined independently of L.

Furthermore, the integrated correlations depend on distances separating the surfaces and volumes over which they are integrated. Let ρ be the radius of the smallest sphere containing the volumes and surfaces over which the correlations are integrated and define $\tilde{\rho} = \rho/\Delta$. Then the integrals can be written in the following forms

$$\tilde{I}^1 = \tilde{I}^{10}\tilde{\rho} \tag{2.35}$$

$$\tilde{I}^2 = \tilde{I}^{20} + (\lambda\tilde{\rho})^{2/3}\tilde{I}^{21} \tag{2.36}$$

$$\tilde{I}^3 = \tilde{I}^{30}\tilde{\rho} \tag{2.37}$$

$$\tilde{I}^4 = \tilde{I}^{40} + (\lambda\tilde{\rho})^{2/3}\tilde{I}^{41} + (\lambda\tilde{\rho})^{4/3}\tilde{I}^{42} \tag{2.38}$$

$$\tilde{I}^5 = \tilde{I}^{50} + (\lambda\tilde{\rho})^{2/3}\tilde{I}^{51} + (\lambda\tilde{\rho})^{4/3}\tilde{I}^{52}. \tag{2.39}$$

Given the expressions for $I^{\alpha\beta}$ stated above, the expressions for $\tilde{I}^{\alpha\beta}$ are easily deduced.

2.5. *Estimation of kinetic energy and dissipation rate*

Equations (2.17) and (2.22) depend on estimates of the turbulent kinetic energy and its dissipation rate.

The turbulent kinetic energy is estimated from filtered data as

$$k \approx \frac{1}{2}\langle w_i w_i \rangle. \tag{2.40}$$

The justification for this approximation is that most of the energy is contained in the large scales. The variance is deduced from $u^2 = 2k/3$.

Two approaches to estimating the dissipation rate were investigated. The first approach is based on the observation that $\tilde{I}^2$ can be computed from

$$\tilde{I}^2_{lj}(v', v) = \frac{\langle w_l(\mathbf{x}')w_j(\mathbf{x})\rangle}{u^2}, \tag{2.41}$$

which gives, on substitution into (2.36),

$$\frac{\langle w_l(\mathbf{x}')w_j(\mathbf{x})\rangle}{u^2} = \tilde{I}^{20}_{lj} + (\lambda\tilde{\rho})^{2/3}\tilde{I}^{21}_{lj}. \tag{2.42}$$

Contracting and using the definitions of $\tilde{\rho}$ and λ leads to

$$\epsilon = \frac{1}{\rho}\left(\frac{\langle w_l(\mathbf{x}')w_l(\mathbf{x})\rangle - u^2\tilde{I}^{20}_{ll}}{\tilde{I}^{21}_{ll}}\right)^{3/2}. \tag{2.43}$$

Since ρ, $\tilde{I}^{20}$, and $\tilde{I}^{21}$ are specified by the geometric configuration of the cells over which the integrals are evaluated, ϵ as given by (2.43) is a function only of the variance and the two-point second-order correlation. The accuracy of (2.43) was evaluated *a priori* on a 32^3 grid using a single filtered velocity field of a DNS of forced isotropic turbulence at $\mathrm{Re}_\lambda = 164$. Figure 1 demonstrates that reasonably accurate approximations can be obtained if $r^1/\Delta > 3$, keeping in mind that (2.43), based on the assumption of an infinite Reynolds number, cannot be expected to reproduce the dissipation rate of the DNS exactly. It is worth noting that (2.43) exhibits the correct dynamic behavior because it can be shown that $\langle w_l(\mathbf{x}')w_l(\mathbf{x})\rangle = u^2\tilde{I}^{20}_{ll}$ for uniform flow fields, and hence the dissipation vanishes as required.

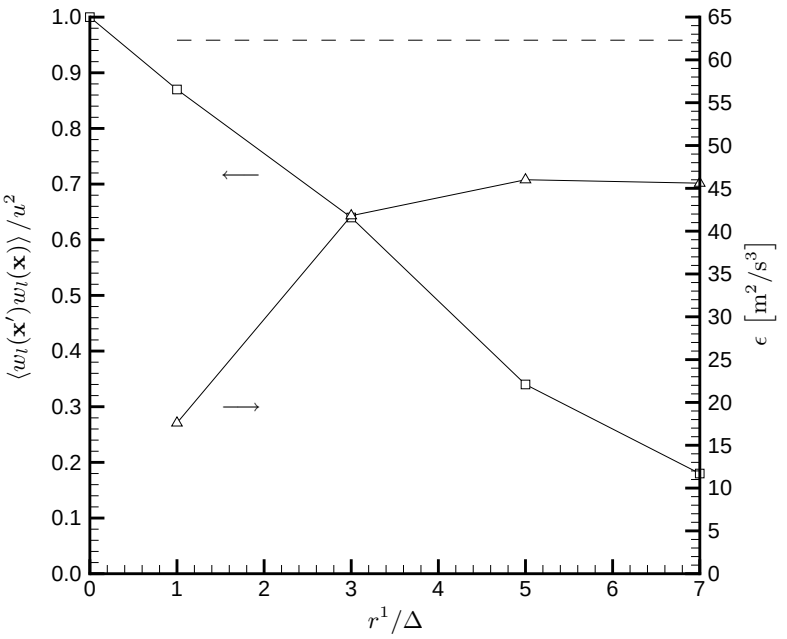

FIGURE 1. Behavior of correlation coefficient and dissipation-rate estimate given by (2.43) with non-dimensional separation distance r^1/Δ. – – – – : Dissipation rate from filtered DNS of forced isotropic turbulence, □ : computed correlation coefficient $\langle w_l(\mathbf{x}')w_l(\mathbf{x})\rangle / u^2$, △ : estimated dissipation rate ϵ.

The second approach to estimating the dissipation rate is based on the relation

$$\epsilon \propto \frac{k^{3/2}}{\ell}, \tag{2.44}$$

where ℓ is a length scale of the large-scale motion.

3. Computational approach

In the present work, the optimal-LES method was implemented in a compressible unstructured-grid code based on the cell-centered finite-volume method. The unstructured code allows for grids composed of arbitrary combinations of tetrahedra, prisms, pyramids, and hexahedra, but only uniform hexahedral grids are considered in this study.

3.1. *Implementation of optimal-LES method on unstructured grids*

The implementation of the optimal-LES method on unstructured grids consists of three steps. The first step involves the construction of the stencils at each face. For stencils of only two cells per face an explicit construction is not necessary, because these cells can be obtained from the face-to-cell list used in the flux computation. If the stencils are to contain $n > 2$ cells, an Octree-based approach, see, e.g., Knuth (1998), is used to determine a set of candidate cells. The candidate cells are sorted by increasing distance from the face centroid and the closest n cells are chosen. Furthermore, stencil shapes

can be influenced depending on local cell topologies. For example, by considering the scalar product of the face normal vector and the position vector between candidate cell centroids and the face centroid, locally one-dimensional stencils may be constructed.

In the second step, the integrated correlations are evaluated using cubature. This entails the evaluation of d-dimensional integrals of tensor functions of order p. Given the restriction to hexahedral cells in the present work, the DCUHRE package of Berntsen *et al.* (1991) is used for the cubature. The computational cost of evaluating the integrals can be reduced by taking into account the symmetries of the tensors, as well as additional symmetries which arise if two or more cells coincide. On non-deforming grids, the first two steps can be completed in a preprocessing phase.

The third step concerns the actual determination of the stencil weights during a computation. This involves the estimation of the turbulence kinetic energy and its dissipation rate as described in subsection 2.5, after which the integrated correlations $\tilde{I}^{\alpha\beta}$ are computed from (2.35)-(2.39). The stencil weights follow by solving the linear system given by (2.33) and (2.34), and using (2.31) and (2.32). The fluxes are then determined from (2.3).

3.2. *Numerical method*

The Navier-Stokes equations are integrated in time using the classical fourth-order accurate Runge-Kutta method. The viscous fluxes are computed using face-gradients calculated from a least-squares reconstruction. The optimal-LES approach is applied only to the momentum equations; the continuity and energy equations are approximated with a centered discretization.

Because we simulate the decay of incompressible isotropic turbulence using the compressible Navier-Stokes equations, dilatation damping is employed to prevent density fluctuations from contributing significantly to the turbulent kinetic energy. This is achieved by modifying the viscosity multiplying the divergence in the stress tensor,

$$\tau_{ij} = 2\mu S_{ij} - \frac{2}{3}(\mu + \mu^*)\frac{\partial u_k}{\partial x_k}\delta_{ij}, \tag{3.1}$$

where μ is the dynamic viscosity, S_{ij} is the strain tensor, and μ^* is the additional viscosity used to damp acoustic waves. A value of $\mu^* = 10\mu$ is used in this study.

4. Results and discussion

The decay of isotropic incompressible turbulence was chosen for the preliminary verification of the optimal-LES approach based on the theory of isotropic turbulence. The calculation domain is a cube of edge length 2π discretized with 32^3 cells.

4.1. *Illustration of stencil weights*

It is instructive to briefly describe the stencils obtained using the finite-volume optimal-LES approach. Using the abbreviations introduced by Langford (2000), namely

$$\widetilde{w^2} = \frac{1}{2}\left[\left(w^+\right)^2 + \left(w^-\right)^2\right] \quad \text{and} \quad \overline{w^2} = w^+ w^-,$$

where the superscripts denote the cells as indicated in figure 2, an approximation of the normal momentum flux can be expressed as

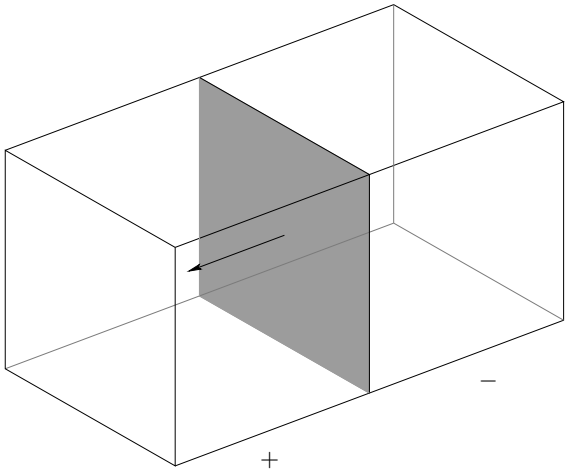

FIGURE 2. Illustration of cell configuration for stencil of two hexahedral cells. The arrow indicates the direction of the face-normal vector.

$$\frac{1}{\Delta^2}\int_s u_1^2\,d\mathbf{x} = 1.2674\,\widetilde{w_1^2} + 0.4750\,\overline{w_1^2} + 0.4200\left(\widetilde{w_2^2} + \widetilde{w_3^2}\right) - 0.0036\left(\overline{w_2^2} + \overline{w_3^2}\right) - 0.1903\,\frac{w_1^+ - w_1^-}{\Delta},$$

and an approximation of the tangential momentum flux is given by

$$\frac{1}{\Delta^2}\int_s u_2u_1\,d\mathbf{x} = 1.9468\left(\frac{w_1^+ + w_1^-}{2}\right)\left(\frac{w_2^+ + w_2^-}{2}\right) - 0.0840\left(w_1^-w_2^+ + w_1^+w_2^-\right) - 0.0785\,\frac{w_2^+ - w_2^-}{\Delta}.$$

For comparison, note that the traditional finite-volume schemes used for LES computations would probably employ a purely-centered approximation given by, for example,

$$\frac{1}{\Delta^2}\int_s u_1^2\,d\mathbf{x} = 0.5000\,\widetilde{w_1^2} + 0.5000\,\overline{w_1^2},$$

and

$$\frac{1}{\Delta^2}\int_s u_2u_1\,d\mathbf{x} = \left(\frac{w_1^+ + w_1^-}{2}\right)\left(\frac{w_2^+ + w_2^-}{2}\right).$$

The most obvious difference is that the optimal-LES stencils are not consistent. As stated in subsection 2.1, the requirement of consistency does not apply to LES because the cells are not small compared to the characteristic length scales of the turbulence. Furthermore, consistency is irrelevant because the stencil weights include the model term. The diffusive contribution to the fluxes is due to the linear term in (2.3). Langford (2000) discussed finite-volume optimal-LES stencils in detail.

4.2. *Simulation of decaying isotropic turbulence*

Before we turn to a presentation and discussion of the results, two issues merit special attention. The first issue concerns the dynamic computation of $\tilde{I}^3$ using (2.24). We have

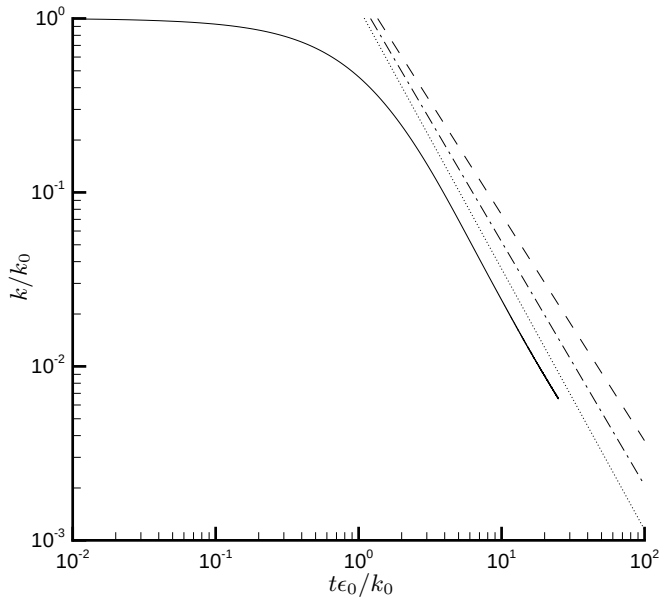

FIGURE 3. Behavior of normalized turbulent kinetic energy with normalized time. ——— : Optimal-LES result, – – – – : decay-law exponent $n = 1.3$, —·— : decay-law exponent $n = 1.4$, ····· : decay-law exponent $n = 1.5$.

thus far been unable to evaluate $\tilde{I}^3$ accurately using spatial averaging; it was not possible to discern a non-zero entry pattern reliably. The present results have therefore been obtained by setting $\tilde{I}^3 = 0$. We will revisit the dynamic computation of $\tilde{I}^3$ in the future.

The second issue is the estimation of the dissipation rate. The use of (2.43) leads to rapid growth of turbulent kinetic energy after an initial period of decay. Although the dissipation rate increased in conjunction with the growth of kinetic energy, the increase appeared to be too slow to prevent blow-up. Hence it seems that the coupling of the dissipation rate given by (2.43) to the turbulent kinetic energy is too weak. To proceed with the preliminary investigation, we have thus used (2.44) with a constant of proportionality $C = 10$ and $\ell = 2\pi$. A constant length scale is obviously a crude approximation to the growth of the integral length scale as the turbulence decays, but sufficient for this preliminary investigation. The large value of the coefficient is a consequence of the definition of ℓ.

The decay of the normalized turbulence kinetic energy and its dissipation rate is depicted in figures 3 and 4, in which the abscissae are given by the physical time normalized by the eddy-turnover time at $t = 0$. For comparison, the decay rates given by the respective analytical decay laws are indicated. It can be seen that the decay rates of both quantities are close to the typical values of the decay-law exponents after an initial adjustment period. The decay rate of the dissipation rate exhibits a gradual change toward the end of the simulation, which we attribute to the choice of a constant length scale.

The three-dimensional energy spectrum at $t\epsilon_0/k_0 = 5.6$ is depicted in figure 5. The pronounced roll-off at high wavenumbers is unexplained at present. Separate investigations have established that the roll-off is not influenced by the physical viscosity or the additional viscosity coefficient used for dilatation damping.

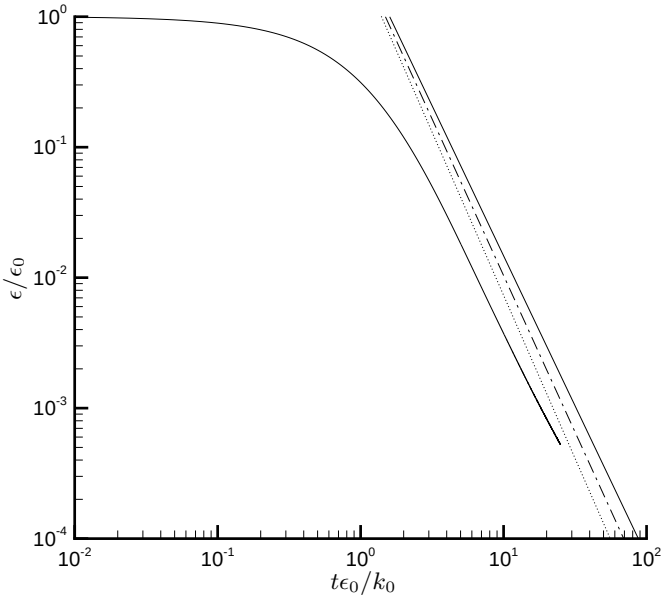

FIGURE 4. Behavior of normalized dissipation rate with normalized time. ——— : Optimal-LES result, - - - - : decay-law exponent $n = 2.3$, —·— : decay-law exponent $n = 2.4$, ····· : decay-law exponent $n = 2.5$.

5. Conclusions and further work

A new method of determining the correlations required by the optimal-LES approach has been presented. The new approach is based on Kolmogorov's theory for isotropic turbulence and leads to stencil coefficients which are determined from integrated multi-point correlations. By using this approach, the explicit dependence of the optimal-LES method on DNS data is eliminated and the applicability is extended to high-Reynolds-number flows in complex geometries.

The new optimal-LES method was implemented in an unstructured finite-volume code. A preliminary verification for decaying isotropic turbulence gave satisfactory results for decay rates of the turbulence kinetic energy and its dissipation rate. The three-dimensional energy spectrum indicates that further work is required.

Further work will include the following:

- An investigation of the reasons for the pronounced roll-off in the three-dimensional energy spectrum at high wavenumbers.
- An analysis of (2.43) using DNS data.
- An investigation into averaging techniques which allow a robust and accurate dynamic determination of $\tilde{I}^3$.
- An extension of the evaluation of the integrated correlation to arbitrary unstructured grids including tetrahedral, prismatic, and pyramidal cells.
- An analysis of the accuracy of the isotropic approximations in inhomogeneous flows.
- An extension of the finite-volume optimal-LES approach to compressible flows, for which an approximation of the mass flux and correlations involving the pressure and temperature are required.

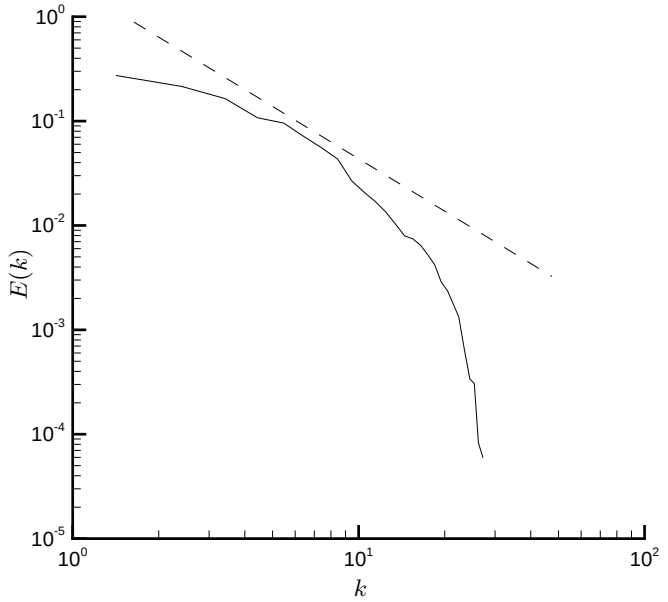

FIGURE 5. Three-dimensional energy spectrum at $t\epsilon_0/k_0 = 5.6$. □ : Optimal-LES result, – – – – : $k^{-5/3}$.

Acknowledgments

The first author would like to acknowledge helpful discussions with Mr. Paulo Zandonade, Dr. Ramesh Balakrishnan, and Mr. Sofiane Benhamadouche. The first author is funded by the Department of Energy through the University of California under Subcontract number B341494.

REFERENCES

ADRIAN, R. 1995 Stochastic estimation of the structure of turbulent fields. *Theor. and Appl. Mech. Dept., Univ. of Illinois at Urbana–Champaign,* Tech. Rept. No. 800.

BALAKRISHNAN, R. AND MOSER, R.D. 2001 Optimal finite-volume stencils for large-eddy simulation of high Re turbulence. *Bull. Am. Phys. Soc.*, **46**(10), 159-160, 2001.

BERNTSEN, J., ESPELID T.O., AND GENZ A. Algorithm 698: DCUHRE: An adaptive multidimensional integration routine for a vector of integrals, *ACM Trans. Math. Softw.*, **17**(4),452-456. Software available from: `http://www.sci.wsu.edu/math/faculty/genz/homepage`.

KNUTH, D.E. 1998 *The Art of Computer Programming, Vol. 3, Sorting and Searching*, Addison Wesley.

LANGFORD, J. 2000 Toward ideal large-eddy simulation. *Ph.D. Thesis*, Univ. of Illinois at Urbana–Champaign.

LANGFORD, J. AND MOSER, R.D. 1999 Optimal LES formulations for isotropic turbulence. *J. Fluid Mech.*, **398**, 321-346.

VÖLKER, S. 2000 Optimal large-eddy simulation of turbulent channel flow. *Ph.D. Thesis*, Univ. of Illinois at Urbana–Champaign.